

Non-Hermitian Chern bands and Chern numbers

Shunyu Yao,¹ Fei Song,¹ and Zhong Wang^{1,2,*}

¹*Institute for Advanced Study, Tsinghua University, Beijing, 100084, China*

²*Collaborative Innovation Center of Quantum Matter, Beijing, 100871, China*

The relation between chiral edge modes and bulk Chern number is a paradigmatic example of bulk-boundary correspondence. We show that in the presence of non-Hermiticity, the Chern number defined by the Bloch Hamiltonian is not strictly tied to the chiral edge modes. We introduce a non-Bloch Chern number for non-Hermitian Chern bands, which faithfully counts the chiral edge modes. The theory is backed up by the open-boundary energy spectra and dynamics of a concrete lattice model, whose phase diagram is found to be consistent with the theoretical prediction. Our results highlight a unique and essential feature of non-Hermitian bands.

The Hamiltonian is always Hermitian in the standard quantum mechanics. Nevertheless, non-Hermitian Hamiltonians[1, 2] are highly useful and efficient in describing many phenomena in nature, such as various open systems[3–12] and waves propagations with gain and loss[13–39]. Recently, topological phenomena in non-Hermitian systems have attracted considerable attentions. For example, it has been proposed that electron’s non-Hermitian self energy, which stems from disorder scatterings or e-e interactions[40–42], can generate novel topological effects such as bulk Fermi arcs[40, 41] (more recently, this effect has been observed in photonic crystals[43]). The interplay between non-Hermiticity and topology has been a growing field with a host of interesting theoretical[44–74] and experimental[75–81] progresses witnessed in recent years.

A central principle of topological states is the bulk-boundary (or bulk-edge) correspondence, which asserts that the robust boundary states are tied to the bulk topological invariants. Within the band theory, the bulk topological invariants are defined using the Bloch Hamiltonian[82–85]. This has been well understood in the usual context of Hermitian Hamiltonians; nevertheless, it a subtle issue to generalize bulk-boundary correspondence to non-Hermitian systems[44–52]. As demonstrated numerically[46, 49, 50, 52], the bulk spectrum of a one-dimensional (1D) open-boundary system can be remote from that of the corresponding closed system. Furthermore, through the 1D non-Hermitian Su-Schrieffer-Heeger (SSH) model with a chiral symmetry (Class AIII[84]), it has been shown[52] that topological invariants defined by the Bloch Hamiltonian[46–48] are not strictly related to the topological edge modes, in sharp contrast to Hermitian cases. It represents a breakdown of the usual bulk-boundary correspondence, nevertheless, a generalized correspondence is valid via the “non-Bloch topological invariant”, which tells the presence or absence of edge zero modes[52].

The topology of the 1D model requires an additional chiral symmetry to stabilize, which is often fragile in real systems. In 2D, Chern bands are robust in the absence of symmetries (i.e., being “purely topological”). Non-Hermitian Chern bands are relevant to a number of physical systems (e.g., photonic systems[37], topological-insulator lasers[74, 86]). In an interesting recent work[44], four equivalent Chern numbers (“left/right-left/right”) have been introduced for non-

Hermitian Bloch bands.

In this work, we uncover an unexpected bulk-boundary correspondence of non-Hermitian Chern bands. We find that the edge-state phase diagrams of non-Hermitian systems are qualitatively different from the predictions by Chern numbers of Bloch Hamiltonian. This phenomenon is attributed to the non-Bloch-wave character of non-Hermitian bands in the presence of a boundary (edge). Furthermore, we introduce a “non-Bloch Chern number”, which is strictly tied to the number of chiral edge modes. As an illustration, we study a concrete lattice model, whose energy spectra and dynamics (edge wave propagations) support our theory.

Model.—We consider a square-lattice model, with the Bloch Hamiltonian given as[44]

$$H(\mathbf{k}) = (v_x \sin k_x + i\gamma_x)\sigma_x + (v_y \sin k_y + i\gamma_y)\sigma_y + (m - t_x \cos k_x - t_y \cos k_y + i\gamma_z)\sigma_z, \quad (1)$$

where $\sigma_{x,y,z}$ are Pauli matrices. The Hermitian part is the Qi-Wu-Zhang model[87](a variation of Haldane model[88]); the non-Hermitian effects are parameterized by $\gamma_{x,y,z}$, which appears as “imaginary Zeeman fields”[89]. Without non-Hermiticity ($\gamma_{x,y,z} = 0$), we have a topological transition point at $m = t_x + t_y$, where the Chern number jumps between 0 and 1. We shall focus on m being close to $t_x + t_y$ ($\gamma_{x,y,z}$ are taken to be small compared to $t_{x,y}$). The eigenvalues of $H(\mathbf{k})$ are

$$E_{\pm}(\mathbf{k}) = \pm \sqrt{\sum_{i=x,y,z} (h_i^2 - \gamma_i^2 + 2i\gamma_i h_i)}, \quad (2)$$

where $(h_x, h_y, h_z) = (v_x \sin k_x, v_y \sin k_y, m - \sum_i t_i \cos k_i)$. Those \mathbf{k} with $|E_{\pm}(\mathbf{k})| = 0$ are referred to as gapless points. They are also exceptional points in the \mathbf{k} space, and the eigenstates of $H(\mathbf{k})$ are exchanged along a contour encircling one of these points[44]. As model parameters are tuned, the gapless points can be created or annihilated in pairs in \mathbf{k} space. The phase boundaries separating the gapped and gapless regions are located at $m = m_{\pm}$, which has a simple expression when $\gamma_z = 0$:

$$m_{\pm} = t_x + t_y \pm \sqrt{\gamma_x^2 + \gamma_y^2}. \quad (3)$$

It is not difficult to find that the $H(\mathbf{k})$ -based Chern number[44] (Bloch Chern number) is 0 for $m > m_+$, 1 for $m < m_-$, and becomes ill-defined in the gapless region $m \in [m_-, m_+]$.

Open boundary.—According to the usual bulk-boundary-correspondence scenario, the chiral edge states of an open-boundary system should be consistent with the Bloch phase diagram outlined above. The Bloch Chern number predicts that chiral edge states should be present for $m < m_-$, and absent for $m > m_+$.

Remarkably, our numerical calculations reveal a different physical picture. To be concrete, let us take $\gamma_z = 0$ and focus on the x - y -symmetric cases, namely $v_x = v_y = v$, $t_x = t_y = t$, $\gamma_x = \gamma_y = \gamma$. We fix $v = t = 1$ and solve the real-space lattice Hamiltonian on a square geometry with edge length L , taking (m, γ) as the varied parameters. We highlight the following findings based on numerical results:

(i) The open-boundary spectrum is entirely different from that of Bloch Hamiltonian. Notably, the open-boundary spectrum is real for the present model. This is in sharp contrast to the Bloch Hamiltonian, whose spectra are complex-valued [see Eq.(2)]. As such, for this specific model, the reality of spectrum is a simplest manifestation of the difference between the open-boundary spectra and Bloch-Hamiltonian spectra (i.e., periodic-boundary spectra). In other models, it is often the case that both Bloch and open-boundary spectra are complex (e.g., this is so when γ_z is nonzero), though other differences between these two spectra remain pronounced.

In addition to the numerical evidence, the reality of square-geometry spectra can be proved as follows. To avoid lengthy notations, let us simply take $L = 2$ to illustrate the proof. Let us order the four sites as $(x, y) = (1, 1), (2, 1), (1, 2), (2, 2)$, and the real-space Hamiltonian reads

$$H = \begin{pmatrix} M & T_x & T_y & 0 \\ T_x^\dagger & M & 0 & T_y \\ T_y^\dagger & 0 & M & T_x \\ 0 & T_y^\dagger & T_x^\dagger & M \end{pmatrix} \quad (4)$$

where

$$M = m\sigma_z + i\gamma_x\sigma_x + i\gamma_y\sigma_y, \\ T_x = -\frac{t_x}{2}\sigma_z - i\frac{v_x}{2}\sigma_x, \quad T_y = -\frac{t_y}{2}\sigma_z - i\frac{v_y}{2}\sigma_y. \quad (5)$$

This Hamiltonian is “ η -pseudo-Hermitian”[90, 91] (not PT -symmetric[38, 55]), namely, it satisfies $\eta^{-1}H^\dagger\eta = H$ with

$$\eta = \begin{pmatrix} 0 & 0 & 0 & \sigma_z \\ 0 & 0 & \sigma_z & 0 \\ 0 & \sigma_z & 0 & 0 \\ \sigma_z & 0 & 0 & 0 \end{pmatrix}. \quad (6)$$

The pseudo-Hermiticity guarantees that for a given eigenstate $|\psi_j\rangle$, i.e., $H|\psi_j\rangle = E_j|\psi_j\rangle$, one can prove $E_j\langle\psi_j|\eta|\psi_j\rangle = E_j^*\langle\psi_j|\eta|\psi_j\rangle$, which indicates $E_j = E_j^*$ unless $\langle\psi_j|\eta|\psi_j\rangle = 0$ [90, 91] (in our case, we have numerically checked that $\langle\psi_j|\eta|\psi_j\rangle \neq 0$).

The distinction between open-boundary and closed-boundary spectra has also been known in a 1D model[46, 49, 50, 52], where the reality of open-boundary spectra becomes most transparent via a similarity transformation, which

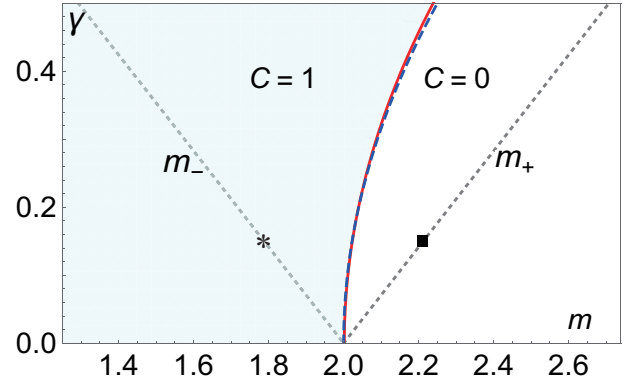


FIG. 1. Topological phase diagram based on the spectra on a square (for $v_{x,y} = t_{x,y} = 1$, $\gamma_{x,y} = \gamma$, $\gamma_z = 0$). Chiral edge states are found in the shadow area, which is therefore topologically nontrivial. The trivial-nontrivial phase boundary is shown as the red solid curve, which is well approximated by the theoretical curve in Eq.(7) (shown as the blue dashed line, which is very close to the red solid curve). Away from this phase boundary, the spectra of square are gapped. The Bloch-Hamiltonian phase boundaries are shown as the dotted lines, whose equations are $m = m_\pm$ with $m_\pm = 2 \pm \sqrt{2}\gamma$. The Bloch-Hamiltonian spectra are gapless for $m \in [m_-, m_+]$. The non-Bloch Chern number C is defined in Eq.(13) (We take the $E_\alpha < 0$ band and omit the α index; see text).

ensures that the spectra are the same as those of an associated Hermitian Hamiltonian[52]. Such a transformation is absent in the present 2D model, which is therefore a more pronounced example of open-closed distinction.

(ii) The open-boundary topological phase transitions, where the chiral edge modes are created or annihilated into the bulk spectra, do not occur at the Bloch phase boundary at m_\pm [Eq.(3)]. By scanning the gap closing points, we find that the edge-state phase boundary is a single curve (red solid one in Fig.1), in sharp contrast to the two straight lines $m = m_\pm$ obtained from the Bloch-Hamiltonian. Furthermore, the numerical phase boundary can be well approximated by the theoretical prediction (to be introduced shortly):

$$m = 2 + \gamma^2. \quad (7)$$

As an illustration of the phase diagram, we show in Fig. 2 the numerical spectra for two values of parameters indicated as \blacksquare and $*$ in Fig.1. Both \blacksquare and $*$ are taken at the Bloch phase boundary where the Bloch Hamiltonian is gapless. Remarkably, the spectra at \blacksquare clearly display an energy gap ≈ 0.4 . A similar bulk gap is found for the $*$ point; in addition, unlike \blacksquare , there are a few in-gap energies, which can be identified as those of chiral edge modes. The absence/existence of chiral edge modes can also be detected by wave packet motions (Fig.2, right panels). In Fig.2(a), there is no chiral edge modes, and the initial wavefunction are superpositions of bulk eigenstates, therefore the wave packet quickly enters into the bulk; in Fig.2(b), one can see clear signature of chiral motions along the edge.

Non-Bloch Chern number.—To understand the underlying physics, let us seek clues in the behaviors of bulk eigen-

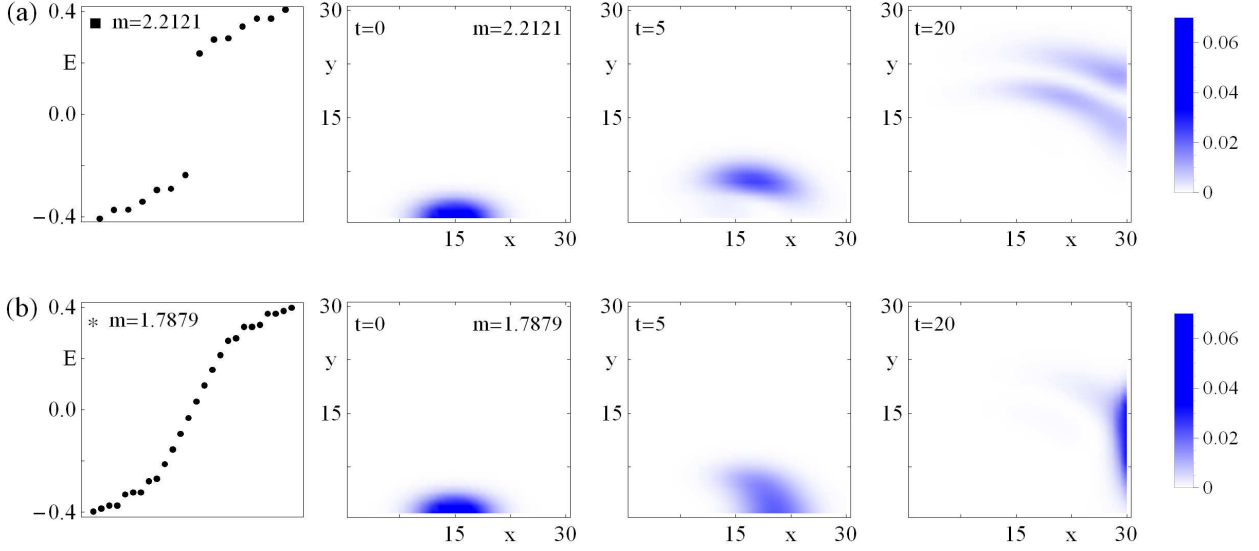


FIG. 2. The lowest energy eigenvalues of a square geometry with $L = 30$ (left panel), and the wave-packet evolution (right three panels). (a) $m = 2.2121$ and (b) $m = 1.7879$ (indicated by \blacksquare and $*$ in Fig.1), with $\gamma = 0.15$ for both. For the energy spectra, a gap is apparent in (a); while in (b), there are a few in-gap edge-state energies. For the wave-packet evolution, the initial wave packet takes the Gaussian form $|\psi(t=0)\rangle = \mathcal{N} \exp[-(x-15)^2/40 - (y-1)^2/10](1, -1)^T$, \mathcal{N} being the normalization factor, and evolves according to the Schrodinger equation $i\partial_t|\psi(t)\rangle = H|\psi(t)\rangle$. The normalized wavefunction $|\psi(t)\rangle / \sqrt{\langle\psi(t)|\psi(t)\rangle}$ is shown for $t = 0, 5, 20$. The wavefunction weight quickly goes into the bulk for (a), while the chiral (unidirectional) motion along the edge is appreciable in (b).

states. Interestingly, we find that all bulk eigenstates are localized near a corner of the square[92]. Furthermore, focusing on the low-energy eigenstates, we find that their spatial decay can be well fitted by $\exp[(\gamma_x/v_x)x + (\gamma_y/v_y)y]$. Accordingly, the low-energy bulk eigenstates are superpositions of “exponentially-modulated Bloch waves” of the form $\exp[(\gamma_x/v_x)x + (\gamma_y/v_y)y] \exp(i\tilde{k}_x x + i\tilde{k}_y y) |u_\alpha(\tilde{k}_x, \tilde{k}_y)\rangle$, $\tilde{k}_{x,y}$ being real and $|u_\alpha(\tilde{k}_x, \tilde{k}_y)\rangle$ being a two-component wavefunction. Therefore, to describe the open-boundary system, we should take the following substitution in the Bloch Hamiltonian [Eq.(1)]:

$$k_i \rightarrow \tilde{k}_i - i\delta_i(\tilde{\mathbf{k}}) \quad (8)$$

where both \tilde{k}_i and $\delta_i(\tilde{\mathbf{k}})$ are real-valued, and $\delta_i(\tilde{\mathbf{k}})$ takes the simple form $\delta_i = \gamma_i/v_i$ for the present model. Since we only focus on low-energy physics, which is sufficient to determine the phase boundary, we take the continuum limit of Eq.(1) by the replacements $\sin k_i \rightarrow k_i$ and $\cos k_i \rightarrow 1 - k_i^2/2$:

$$H(\mathbf{k}) = (v_x k_x + i\gamma_x)\sigma_x + (v_y k_y + i\gamma_y)\sigma_y + (m - t_x - t_y + \frac{t_x}{2}k_x^2 + \frac{t_y}{2}k_y^2)\sigma_z, \quad (9)$$

where we have let $\gamma_z = 0$ for simplicity. After the replacement $k_i \rightarrow \tilde{k}_i - i\gamma_i/v_i$ explained above, the “non-Bloch” continuum Hamiltonian is

$$\tilde{H}(\tilde{\mathbf{k}}) = v_x \tilde{k}_x \sigma_x + v_y \tilde{k}_y \sigma_y + (\tilde{m} + \frac{t_x}{2} \tilde{k}_x^2 + \frac{t_y}{2} \tilde{k}_y^2) \sigma_z, \quad (10)$$

where we have discarded a small $-i \sum_{i=x,y} t_i \gamma_i \tilde{k}_i / v_i \sigma_z$ term, which is not important to determining the phase boundary;

and crucially,

$$\tilde{m} = m - t_x - t_y - \frac{t_x \gamma_x^2}{2v_x^2} - \frac{t_y \gamma_y^2}{2v_y^2}. \quad (11)$$

The spectra of Eq.(10) are real, being consistent with the numerical spectra on the square.

The above approach is quite general and can in principle be implemented directly on lattice models. The general form of Eq.(8) remains applicable, where the decay factors $\delta_i(\mathbf{k})$'s should be obtained numerically or analytically. A non-Bloch Chern number can be introduced via the non-Bloch Hamiltonian $\tilde{H}(\tilde{\mathbf{k}})$, which is generally non-Hermitian. We can define the standard right/left eigenvectors as follows:

$$\tilde{H}(\tilde{\mathbf{k}})|u_{R\alpha}\rangle = E_\alpha|u_{R\alpha}\rangle, \quad \tilde{H}^\dagger(\tilde{\mathbf{k}})|u_{L\alpha}\rangle = E_\alpha^*|u_{L\alpha}\rangle, \quad (12)$$

where α is the band index. In fact, one can diagonalize $\tilde{H}(\tilde{\mathbf{k}})$ as $\tilde{H} = T J T^{-1}$, then every column of T (or $(T^\dagger)^{-1}$) is a right (or left) eigenvector, and the normalization $\langle u_{L\alpha} | u_{R\beta} \rangle = \delta_{\alpha\beta}$ is automatically satisfied. This is followed by the standard definition of projection operator: $P_\alpha(\tilde{\mathbf{k}}) = |u_{R\alpha}(\tilde{\mathbf{k}})\rangle \langle u_{L\alpha}(\tilde{\mathbf{k}})|$. We then introduce the non-Bloch Chern number on the generalized Brillouin-zone torus T^2 parameterized by $\tilde{\mathbf{k}}$:

$$C_{(\alpha)} = \frac{1}{2\pi i} \int_{T^2(\tilde{\mathbf{k}})} d^2 \tilde{\mathbf{k}} \epsilon^{ij} \text{Tr}(P_\alpha \partial_i P_\alpha \partial_j P_\alpha), \quad (13)$$

which can also be expressed in terms of the Berry curvature. The key in this definition is the “generalized Brillouin zone” parameterized by $\tilde{\mathbf{k}}$ instead of the usual Bloch wavevectors \mathbf{k} .

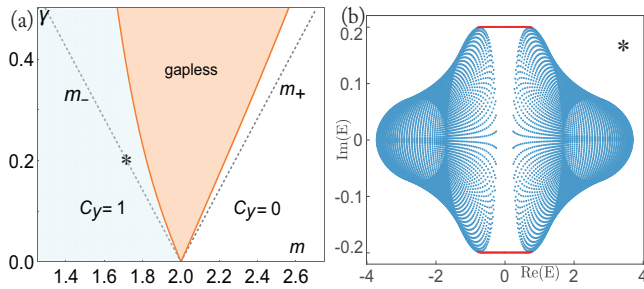


FIG. 3. (a) The “phase diagram” based on the spectra on a cylinder with open boundary condition in the y direction. $t_{x,y} = v_{x,y} = 1$, $\gamma_{x,y} = \gamma$, $\gamma_z = 0$. The dotted lines are the Bloch phase boundaries. (b) The spectra for $(m, \gamma) = (1.717, 0.2)$ (indicated as $*$ in (a)). The length in y direction is $L_y = 40$, and 180 grid points are taken for k_x . The spectra for all k_x 's are shown together in the complex plane, without specifying the k_x value for each data point. The chiral edge states are colored red.

For the present two-band model, the spectra of $\tilde{H}(\tilde{\mathbf{k}})$ are real, and we shall focus on the Chern number of the $E_\alpha < 0$ band, omitting the α index in Eq.(13). We can compute this Chern number from the non-Bloch continuum Hamiltonian Eq.(10), and obtain that $C = 1$ (0) for $\tilde{m} < 0$ (> 0) (Note that the Chern integrand is well-behaved for $\tilde{\mathbf{k}} \rightarrow \infty$ due to the $\tilde{k}_i^2 \sigma_z$ terms). With $t_{x,y} = v_{x,y} = 1$, $\gamma_{x,y} = \gamma$, the topologically-nontrivial condition $\tilde{m} < 0$ becomes $m < 2 + \gamma^2$, and the phase boundary is just Eq.(7). We note that in the low-energy theory, γ is treated as being small, and we can see from Fig.1 that $\gamma = 0.4$ remains well described by it. As a comparison, the Bloch Chern number[44] is nonzero only when $m < 2 - \sqrt{2}\gamma$; moreover, the Bloch Chern number cannot be defined for $m \in [2 - \sqrt{2}\gamma, 2 + \sqrt{2}\gamma]$ because the bands are inseparable[44].

To summarize this approach: One starts from fitting the exponential decay factors of the low-energy states, which are then used to obtain the non-Bloch Hamiltonian $\tilde{H}(\tilde{\mathbf{k}})$. The non-Bloch Chern number is then defined via $\tilde{H}(\tilde{\mathbf{k}})$. Working in the low-energy continuum limit is convenient because of the absence of $\tilde{\mathbf{k}}$ dependence of the decay factors $\delta_{x,y}$. The formulation is conceptually the same if one works directly from the lattice Hamiltonian, though the $\tilde{\mathbf{k}}$ dependence of $\delta_{x,y}$ complicates the calculations. It is desirable to develop efficient algorithm to calculate Eq.(13) directly from the lattice model, which will be left for future studies.

Cylinder.—Now we briefly discuss the cylinder geometry to clarify some potential confusions. Suppose that the cylinder has periodic-boundary condition in the x direction, and open-boundary condition in the y direction. In this geometry, the spectra can be solved as 1D open-boundary systems along the y direction, with the good quantum number k_x taken as a Hamiltonian parameter. As an illustration, let us take a set of parameters indicated as $*$ in Fig.3(a), and show the numerical spectra in Fig.3(b). Chiral edge states can be readily seen in the spectra.

In fact, to characterize the chiral edge states on the cylinder,

one can define a “cylinder Chern number”, which is denoted as C_y because of the open-boundary condition in the y direction. The definition is quite similar to Eq.(13), except that $(\tilde{k}_x, \tilde{k}_y)$ is replaced by (k_x, \tilde{k}_y) , because the eigenstates are forced to be Bloch waves in the x direction. A “cylinder Hamiltonian” $\tilde{H}_y(k_x, \tilde{k}_y)$ can be defined in a manner similar to $\tilde{H}(\tilde{k}_x, \tilde{k}_y)$, and the cylinder Chern number C_y can be defined based on this “cylinder Hamiltonian”, which we shall not repeat due to the resemblance to the construction of C [Eq.(13)].

We would like to emphasize two points: (i) The cylinder Chern number depends on the edge orientation, namely, if we take open-boundary condition in a different direction, the cylinder Chern number can be different. (ii) The original non-Bloch Chern number defined in Eq.(13) is the physically more relevant one. In fact, we have found that the wave-packet motions on the edges of cylinder still follow the phase diagram of Fig.1, namely, chiral edge motions can be detected when C (not C_y) is nonzero. This phenomenon is understandable because a wave packet is quite ignorant of the closed boundary in the x direction if the cylinder circumference is much larger than the wave packet size in the x direction.

Final remarks.—We have shown an unexpected bulk-boundary correspondence that the chiral edge states are determined by a “non-Bloch” Chern number instead of the Bloch ones. There are many open questions ahead. For example, it is worthwhile to study the respective roles of the Bloch and non-Bloch Chern numbers: What aspects of non-Hermitian physics are described by the Bloch/non-Bloch one? In addition, the theory can be generalized by including symmetries. It is also interesting to go beyond the band theory (e.g., to consider interaction effects).

Acknowledgements.—This work is supported by NSFC under grant No. 11674189.

* wangzhongemail@gmail.com

- [1] C. M. Bender, Reports on Progress in Physics **70**, 947 (2007).
- [2] C. M. Bender and S. Boettcher, Physical Review Letters **80**, 5243 (1998).
- [3] I. Rotter, Journal of Physics A: Mathematical and Theoretical **42**, 153001 (2009).
- [4] S. Malzard, C. Poli, and H. Schomerus, Phys. Rev. Lett. **115**, 200402 (2015).
- [5] H. J. Carmichael, Phys. Rev. Lett. **70**, 2273 (1993).
- [6] B. Zhen, C. W. Hsu, Y. Igarashi, L. Lu, I. Kaminer, A. Pick, S.-L. Chua, J. D. Joannopoulos, and M. Soljačić, Nature **525**, 354 (2015).
- [7] S. Diehl, E. Rico, M. A. Baranov, and P. Zoller, Nature Physics **7**, 971 (2011).
- [8] H. Cao and J. Wiersig, Rev. Mod. Phys. **87**, 61 (2015).
- [9] Y. Choi, S. Kang, S. Lim, W. Kim, J.-R. Kim, J.-H. Lee, and K. An, Phys. Rev. Lett. **104**, 153601 (2010).
- [10] P. San-Jose, J. Cayao, E. Prada, and R. Aguado, Scientific reports **6**, 21427 (2016).
- [11] T. E. Lee and C.-K. Chan, Phys. Rev. X **4**, 041001 (2014).
- [12] T. E. Lee, F. Reiter, and N. Moiseyev, Phys. Rev. Lett. **113**, 250401 (2014).

- [13] K. G. Makris, R. El-Ganainy, D. N. Christodoulides, and Z. H. Musslimani, *Phys. Rev. Lett.* **100**, 103904 (2008).
- [14] S. Longhi, *Phys. Rev. Lett.* **103**, 123601 (2009).
- [15] C. E. Rüter, K. G. Makris, R. El-Ganainy, D. N. Christodoulides, M. Segev, and D. Kip, *Nature physics* **6**, 192 (2010).
- [16] S. Klaiman, U. Günther, and N. Moiseyev, *Phys. Rev. Lett.* **101**, 080402 (2008).
- [17] S. Bittner, B. Dietz, U. Günther, H. L. Harney, M. Miski-Oglu, A. Richter, and F. Schäfer, *Phys. Rev. Lett.* **108**, 024101 (2012).
- [18] A. Regensburger, C. Bersch, M.-A. Miri, G. Onishchukov, D. N. Christodoulides, and U. Peschel, *Nature* **488**, 167 (2012).
- [19] A. Guo, G. J. Salamo, D. Duchesne, R. Morandotti, M. Volatier-Ravat, V. Aimez, G. A. Siviloglou, and D. N. Christodoulides, *Phys. Rev. Lett.* **103**, 093902 (2009).
- [20] M. Liertzer, L. Ge, A. Cerjan, A. D. Stone, H. E. Türeci, and S. Rotter, *Phys. Rev. Lett.* **108**, 173901 (2012).
- [21] B. Peng, Ş. Özdemir, S. Rotter, H. Yilmaz, M. Liertzer, F. Monifi, C. Bender, F. Nori, and L. Yang, *Science* **346**, 328 (2014).
- [22] Z. Lin, H. Ramezani, T. Eichelkraut, T. Kottos, H. Cao, and D. N. Christodoulides, *Phys. Rev. Lett.* **106**, 213901 (2011).
- [23] L. Lu, J. D. Joannopoulos, and M. Soljacic, *Nat Photon* **8**, 821 (2014).
- [24] L. Feng, Y.-L. Xu, W. S. Fegadolli, M.-H. Lu, J. E. Oliveira, V. R. Almeida, Y.-F. Chen, and A. Scherer, *Nature materials* **12**, 108 (2013).
- [25] R. Fleury, D. Sounas, and A. Alù, *Nature communications* **6**, 5905 (2015).
- [26] L. Chang, X. Jiang, S. Hua, C. Yang, J. Wen, L. Jiang, G. Li, G. Wang, and M. Xiao, *Nature photonics* **8**, 524 (2014).
- [27] H. Hodaei, A. U. Hassan, S. Wittek, H. Garcia-Gracia, R. El-Ganainy, D. N. Christodoulides, and M. Khajavikhan, *Nature* **548**, 187 (2017).
- [28] H. Hodaei, M.-A. Miri, M. Heinrich, D. N. Christodoulides, and M. Khajavikhan, *Science* **346**, 975 (2014).
- [29] L. Feng, Z. J. Wong, R.-M. Ma, Y. Wang, and X. Zhang, *Science* **346**, 972 (2014).
- [30] K. Kawabata, Y. Ashida, and M. Ueda, *Phys. Rev. Lett.* **119**, 190401 (2017).
- [31] T. Gao, E. Estrecho, K. Bliokh, T. Liew, M. Fraser, S. Brodbeck, M. Kamp, C. Schneider, S. Höfling, Y. Yamamoto, *et al.*, *Nature* **526**, 554 (2015).
- [32] H. Xu, D. Mason, L. Jiang, and J. Harris, *Nature* **537**, 80 (2016).
- [33] Y. Ashida, S. Furukawa, and M. Ueda, *Nature communications* **8**, 15791 (2017).
- [34] W. Chen, Ş. K. Özdemir, G. Zhao, J. Wiersig, and L. Yang, *Nature* **548**, 192 (2017).
- [35] K. Ding, G. Ma, M. Xiao, Z. Q. Zhang, and C. T. Chan, *Phys. Rev. X* **6**, 021007 (2016).
- [36] C. A. Downing and G. Weick, *Phys. Rev. B* **95**, 125426 (2017).
- [37] T. Ozawa, H. M. Price, A. Amo, N. Goldman, M. Hafezi, L. Lu, M. Rechtsman, D. Schuster, J. Simon, O. Zeitlinger, and I. Carusotto, *ArXiv e-prints* (2018), arXiv:1802.04173 [physics.optics].
- [38] R. El-Ganainy, K. G. Makris, M. Khajavikhan, Z. H. Musslimani, S. Rotter, and D. N. Christodoulides, *Nature Physics* **14**, 11 (2018).
- [39] S. Longhi, *ArXiv e-prints* (2018), arXiv:1802.05025 [physics.optics].
- [40] V. Kozii and L. Fu, *ArXiv e-prints* (2017), arXiv:1708.05841 [cond-mat.mes-hall].
- [41] M. Papaj, H. Isobe, and L. Fu, *ArXiv e-prints* (2018), arXiv:1802.00443 [cond-mat.dis-nn].
- [42] H. Shen and L. Fu, *ArXiv e-prints* (2018), arXiv:1802.03023 [cond-mat.str-el].
- [43] H. Zhou, C. Peng, Y. Yoon, C. W. Hsu, K. A. Nelson, L. Fu, J. D. Joannopoulos, M. Soljačić, and B. Zhen, (2018), 10.1126/science.aap9859.
- [44] H. Shen, B. Zhen, and L. Fu, *Phys. Rev. Lett.* **120**, 146402 (2018).
- [45] K. Esaki, M. Sato, K. Hasebe, and M. Kohmoto, *Phys. Rev. B* **84**, 205128 (2011).
- [46] T. E. Lee, *Phys. Rev. Lett.* **116**, 133903 (2016).
- [47] D. Leykam, K. Y. Bliokh, C. Huang, Y. D. Chong, and F. Nori, *Phys. Rev. Lett.* **118**, 040401 (2017).
- [48] S. Lieu, *Phys. Rev. B* **97**, 045106 (2018).
- [49] Y. Xiong, *ArXiv e-prints* (2017), arXiv:1705.06039v1 [cond-mat.mes-hall].
- [50] V. M. Martinez Alvarez, J. E. Barrios Vargas, and L. E. F. Foa Torres, *Phys. Rev. B* **97**, 121401 (2018).
- [51] Z. Gong, Y. Ashida, K. Kawabata, K. Takasan, S. Higashikawa, and M. Ueda, *ArXiv e-prints* (2018), arXiv:1802.07964v1 [cond-mat.mes-hall].
- [52] S. Yao and Z. Wang, *ArXiv e-prints* (2018), arXiv:1803.01876 [cond-mat.mes-hall].
- [53] M. S. Rudner and L. S. Levitov, *Phys. Rev. Lett.* **102**, 065703 (2009).
- [54] S.-D. Liang and G.-Y. Huang, *Phys. Rev. A* **87**, 012118 (2013).
- [55] Y. C. Hu and T. L. Hughes, *Phys. Rev. B* **84**, 153101 (2011).
- [56] J. Gong and Q.-h. Wang, *Phys. Rev. A* **82**, 012103 (2010).
- [57] M. S. Rudner, M. Levin, and L. S. Levitov, *ArXiv e-prints* (2016), arXiv:1605.07652 [cond-mat.mes-hall].
- [58] B. Zhu, R. Lü, and S. Chen, *Phys. Rev. A* **89**, 062102 (2014).
- [59] Z. Gong, S. Higashikawa, and M. Ueda, *Phys. Rev. Lett.* **118**, 200401 (2017).
- [60] X. Wang, T. Liu, Y. Xiong, and P. Tong, *Phys. Rev. A* **92**, 012116 (2015).
- [61] K. Kawabata, Y. Ashida, H. Katsura, and M. Ueda, *ArXiv preprint arXiv:1801.00499* (2018).
- [62] X. Ni, D. Smirnova, A. Poddubny, D. Leykam, Y. Chong, and A. B. Khanikaev, *ArXiv e-prints* (2018), arXiv:1801.04689 [cond-mat.mes-hall].
- [63] A. A. Zyuzin and A. Y. Zyuzin, *Phys. Rev. B* **97**, 041203 (2018).
- [64] A. Cerjan, M. Xiao, L. Yuan, and S. Fan, *Phys. Rev. B* **97**, 075128 (2018).
- [65] M. Klett, H. Cartarius, D. Dast, J. Main, and G. Wunner, *Phys. Rev. A* **95**, 053626 (2017).
- [66] H. Menke and M. M. Hirschmann, *Phys. Rev. B* **95**, 174506 (2017).
- [67] L. Zhou, Q.-h. Wang, H. Wang, and J. Gong, *ArXiv e-prints* (2017), arXiv:1711.10741 [cond-mat.stat-mech].
- [68] J. González and R. A. Molina, *Phys. Rev. B* **96**, 045437 (2017).
- [69] C. Yuce, *Phys. Rev. A* **93**, 062130 (2016).
- [70] W. Hu, H. Wang, P. P. Shum, and Y. D. Chong, *Phys. Rev. B* **95**, 184306 (2017).
- [71] Y. Xu, S.-T. Wang, and L.-M. Duan, *Phys. Rev. Lett.* **118**, 045701 (2017).
- [72] S. Ke, B. Wang, H. Long, K. Wang, and P. Lu, *Optics Express* **25**, 11132 (2017).
- [73] C. Yin, H. Jiang, L. Li, R. Lü, and S. Chen, *ArXiv e-prints* (2018), arXiv:1802.04169v1 [cond-mat.mes-hall].
- [74] G. Harari, M. A. Bandres, Y. Lumer, M. C. Rechtsman, Y. Chong, M. Khajavikhan, D. N. Christodoulides, and M. Segev, *Science*, eaar4003 (2018).

- [75] J. M. Zeuner, M. C. Rechtsman, Y. Plotnik, Y. Lumer, S. Nolte, M. S. Rudner, M. Segev, and A. Szameit, *Phys. Rev. Lett.* **115**, 040402 (2015).
- [76] L. Xiao, X. Zhan, Z. H. Bian, K. K. Wang, X. Zhang, X. P. Wang, J. Li, K. Mochizuki, D. Kim, N. Kawakami, W. Yi, H. Obuse, B. C. Sanders, and P. Xue, *Nature Physics* **13**, 1117 (2017).
- [77] S. Weimann, M. Kremer, Y. Plotnik, Y. Lumer, S. Nolte, K. Makris, M. Segev, M. Rechtsman, and A. Szameit, *Nature materials* **16**, 433 (2017).
- [78] C. Poli, M. Bellec, U. Kuhl, F. Mortessagne, and H. Schomerus, *Nature communications* **6**, 6710 (2015).
- [79] M. Parto, S. Wittek, H. Hodaei, G. Harari, M. A. Bandres, J. Ren, M. C. Rechtsman, M. Segev, D. N. Christodoulides, and M. Khajavikhan, *ArXiv e-prints* (2017), arXiv:1709.00523 [physics.optics].
- [80] H. Zhao, P. Miao, M. H. Teimourpour, S. Malzard, R. El-Ganainy, H. Schomerus, and L. Feng, *ArXiv e-prints* (2017), arXiv:1709.02747 [physics.optics].
- [81] X. Zhan, L. Xiao, Z. Bian, K. Wang, X. Qiu, B. C. Sanders, W. Yi, and P. Xue, *Phys. Rev. Lett.* **119**, 130501 (2017).
- [82] M. Z. Hasan and C. L. Kane, *Rev. Mod. Phys.* **82**, 3045 (2010).
- [83] X.-L. Qi and S.-C. Zhang, *Rev. Mod. Phys.* **83**, 1057 (2011).
- [84] C.-K. Chiu, J. C. Y. Teo, A. P. Schnyder, and S. Ryu, *Rev. Mod. Phys.* **88**, 035005 (2016).
- [85] B. A. Bernevig and T. L. Hughes, *Topological insulators and topological superconductors* (Princeton University Press, Princeton, NJ, 2013).
- [86] M. A. Bandres, S. Wittek, G. Harari, M. Parto, J. Ren, M. Segev, D. N. Christodoulides, and M. Khajavikhan, *Science*, eaar4005 (2018).
- [87] X.L. Qi, Y.S. Wu, and S.C. Zhang, *Phys. Rev. B* **74**, 085308 (2006).
- [88] F. D. M. Haldane, *Phys. Rev. Lett.* **61**, 2015 (1988).
- [89] T. D. Lee and C. N. Yang, *Phys. Rev.* **87**, 410 (1952).
- [90] A. Mostafazadeh, *Journal of Mathematical Physics* **43**, 2814 (2002), math-ph/0110016.
- [91] A. Mostafazadeh, *Journal of Mathematical Physics* **43**, 205 (2002), math-ph/0107001.
- [92] An analogous phenomenon has been seen numerically[50] and analytically[52] in the 1D non-Hermitian SSH model.